GDAŃSK UNIVERSITY OF TECHNOLOGY

TASK Quarterly 29 (2) 2025

Empirical Model of a High-Temperature Proton Exchange Membrane Fuel Cell for Diagnostics Based on the Test Without Active Gases Procedure

Wojciech Aleksander Rosiński[1,*], **Andrzej Wilk**[1], **Szymon Potrykus**[1,2]

[1] Faculty of Electrical and Control Engineering, Gdańsk University of Technology, Narutowicza 11/12, Gdańsk, 80-233, Poland
[2]Advanced Materials Center, Faculty of Electronics, Telecommunications and Informatics, Gdańsk University of Technology, Narutowicza 11/12, Gdańsk, 80-233, Poland

[*]wojciech.rosinski@pg.edu.pl

https://doi.org/10.34808/tq2025/29.2/a

Abstract

This paper presents a static electrical model developed to analyze results from the Test Without Active Gases (TWAG) procedure, which characterizes fuel cell behavior in the absence of electrochemically active gases. The model topology is inspired by electric double-layer supercapacitor circuits and was derived from first principles using Lagrangian formalism. It was validated using five experimental test without active gases discharge curves recorded at temperatures between 40°C and 120°C. Despite its simplicity and low computational cost, the model achieved satisfactory accuracy. The extracted parameters indicate potential for further refinement, such as introducing temperature-dependent components. The approach provides insight into the intrinsic electrochemical properties of high-temperature proton exchange membrane fuel cells in states without active gases and may serve as a foundation for broader diagnostic and modeling applications. Future developments may include extending the RC circuit, incorporating nonlinear elements, or applying the model to other fuel cell technologies. Testing on deliberately degraded cells could also help correlate model parameters with cell health.

Keywords:

fuel cells, diagnostics, empirical model

1. Introduction

The global challenges related to the decarbonization of the economy and energy transition involve maximizing the efficiency of energy from renewable energy sources such as hydrogen technologies. Fuel Cells (FCs), in particular, are seen as key components of future energy systems. Systems using fuel cells are characterized by good efficiency and high gravimetric density of stored energy. Fuel cells offer a low carbon footprint and the ability to integrate with renewable energy sources, making them an attractive solution in sectors such as transport, energy and industry [1–4].

Despite its many advantages, fuel cell technology faces a number of challenges. These include, among others, the need to ensure stable operation in variable operating conditions [5], optimization of production and operating costs [6], the development of mathematical models that enable accurate prediction of cell behavior in various operating scenarios [7, 8], and fault classification and diagnosis [9–11]. Understanding the behavior of fuel cells in the absence of active gases is particularly important, as such conditions may occur, for instance, before system start-up and between operation cycles [12].

This applies to two key cases: diagnosis of new cells before their first start-up and diagnostics of potential defects in the cells operating in the system [13, 14]. In both situations, it is necessary to accurately characterize the behavior of the cell as a passive element [12]. A better understanding and control of the properties of the converters used as a link between the cell and the system can enable more effective identification of defects and a more complete understanding of the dynamics of the system in different operating states [15].

Traditional fuel cell models, based on mass transport equations and electrochemical reactions, often fail to accurately replicate the cell's behavior under certain conditions. In the absence of active gases, classical approaches can produce results suggesting no electrochemical activity, which does not reflect the actual behavior of the system.

In practice, without active gases, a fuel cell exhibits characteristics typical of passive electrical components, in particular capacitance and resistance, which can be explained by the presence of structures like the electrical double layer [16]. The double-layer phenomenon is also present in fuel cells operating with active gases, where its effects are explicitly incorporated into advanced modeling frameworks to achieve a more accurate representation of the cell's dynamic behavior [17].

The double layer is an electrochemical phenomenon in which charge separation occurs at the interface between the electrode and the electrolyte, forming a capacitor-like structure [18]. Due to the phenomenon of a double electric layer and pseudo-capacitance, a fuel cell without active gases behaves similarly to a double-layer supercapacitor.

There are many models in the scientific literature that describe the behavior of fuel cells and supercapacitors [19, 20]. For example, Vetter and Schumacher (2018) [21] present an open implementation of a two-phase proton-conductive membrane fuel cell model that takes into account low-temperature operating conditions and complex transport phenomena. Their work highlights the importance of standardization and the availability of simulation models for the development of fuel cell technology. In turn, Krpan et al. (2021) [22] present a dynamic model of cells, based on the representation of an RC circuit, which can be integrated with software for simulation of power systems, enabling the analysis of cell behavior in various operating scenarios.

In the context of modeling the behavior of fuel cells without active gases, it is important to account for phenomena characteristics of supercapacitors, such as the electric double layer and pseudo capacitance. This approach enables a more accurate representation of the actual behavior of the cell, even under conditions of electrochemical inactivity. Accordingly, this article proposes modeling the fuel cell as a passive electrical component by applying the concept of universal modeling, which allows for a generalized description of various electrochemical systems without the need to explicitly replicate their geometry or detailed physical and chemical properties.

The aim of this paper is to present a model that allows the behavior of a fuel cell without active gases to be described, taking into account the phenomena of the electric double layer and capacitive effects characteristic of supercapacitors. The proposed approach aims not only to better understand the electrochemical properties of fuel cells in their passive state, but also to provide a valuable tool for further optimizing power and energy storage systems.

This paper is structured to present the development, implementation, and validation of the proposed fuel cell model. The Materials and Methods section (2) includes an overview of the model topologies, the derivation of the equivalent circuit model based on existing models of supercapacitors exhibiting double-layer behavior, the parameter identification procedure—including the test without active gases test scenario—and the experimental setup. The Results section (3) presents the outcomes of parameter estimation and model validation using experimental data. Finally, the Conclusions section (4) summarizes the main findings and suggest directions for future model enhancements and applications.

2. Materials and Methods

2.1. Proposed model topology

Based on findings reported in the scientific literature [19–22], a candidate equivalent circuit model is proposed for a high-temperature proton exchange membrane (PEM) fuel cell with no active gases. The main factor considered was the number of RC branches, which correlates directly to the degrees of freedom. Based on this, an initial model with one branch was chosen as, if this model proves to provide adequate representation of the charging and discharge curves, it can be further expanded and made more accurate by adding more RC branches. The single branch model also has an additional advantage as it does not require significant computational power to simulate. Fig. 1 presents the equivalent circuit model analyzed in this study for a high-temperature PEM fuel cell operating in the absence of active gases. The only parameter which was not part of the RC branch, marked in Fig. 1 as R_0, was given the name self-discharge resistance.

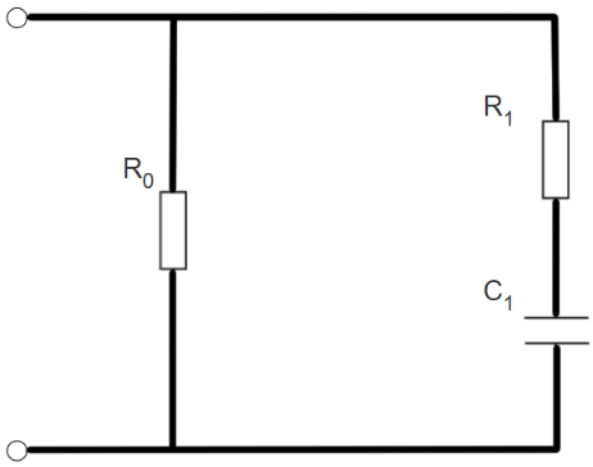

Figure 1: Circuit equivalent model analyzed for a high temperature PEM fuel cell with no active gases present.

2.2. Development of the adopted fuel cell models

Any circuit model equivalent is only a graphical representation of a differential equation system. In this work, a generic model in the form of a system of differential equations of fuel cell in a state without active gases was developed.

The first version of the model that was solved was the model presented in Fig. 2. This model comprises only three lumped elements. In this case, Lagrange's energy method was used to develop equilibrium equations of the model. Lagrange's equation is a unifying technique that involves the energy-state functions for systems (electro-mechanical, electro-chemical) where there is an energy flow between linked systems [23, 24]. The proposed method based on energy quantities can be very useful for development of advanced models of a fuel cell model with no active gases. In the context of the Lagrange method, particularly in circuit analysis, conductance (G) is used instead of resistance (R) because it simplifies calculations and provides a more intuitive representation of how easily current flows through a circuit or component. Conductance is the reciprocal of resistance, meaning a higher conductance signifies easier current flow, while a higher resistance indicates more opposition to current flow.

Lagrange's equation is as follows:

$$\frac{d}{dt}\left(\frac{\partial L(\dot{\xi},\xi)}{\partial \dot{\xi}_k}\right) - \frac{\partial L(\dot{\xi},\xi)}{\partial \xi_k} + \frac{\partial F(\dot{\xi})}{\partial \dot{\xi}_k} = Q_k,$$
$$k = 0, 1, 2, \ldots, n \tag{1}$$

where:

$L\left(\dot{\xi},\xi\right)$ — the Lagrangian of a total system,

$F\left(\dot{\xi}\right)$ — the Rayleigh dissipation function of a total system,

$\dot{\xi}_k$ — the so-called generalized coordinate (degree of freedom),

Q_k — the so-called generalized force,

k — the index of generalized coordinate.

In electrical systems composed exclusively of passive circuit elements such as inductances, capacitances, and resistances, as considered in the present modeling approach, the choice of generalized coordinates depends on the formulation adopted. In the loop (mesh) formulation, generalized coordinates correspond to the currents circulating in the loops and the electrical charges associated with these currents, whereas in the nodal formulation, they are defined in terms of the voltages at network nodes and the associated magnetic flux linkages. Moreover, in pure electrical systems, the notion of generalized forces also takes on a specific interpretation; in the loop formulation, generalized forces are represented by externally applied voltages connected to the electrical loops, while in the nodal formulation, they correspond to external currents injected into the network nodes. This duality reflects fundamental principles of electrical network analysis and provides a rigorous basis for applying variational methods or energy-based techniques in the modeling and simulation of electrical circuits. Fig. 2 presents a single-branch electrical model incorporating one conservative element, namely the capacitance C_1, and two dissipative elements repre-

sented by conductances G_0 and G_1. The circuit is depicted with nodes selected to facilitate analysis using the nodal formulation approach.

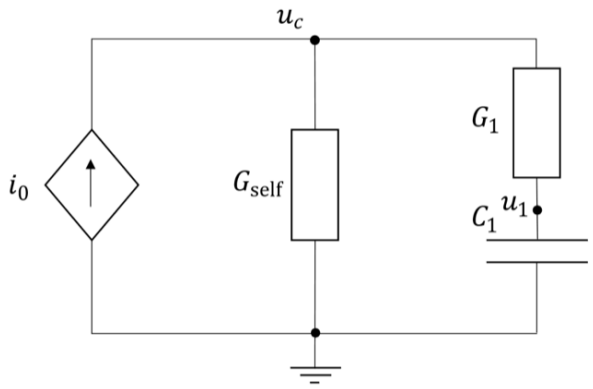

Figure 2: Single-branch model with capacitance C_1 and conductances G_0, G_1 (nodal formulation).

Nodal formulation was chosen to solve the model. The nodal variables chosen are shown in Fig. 2. The Lagrangian and Rayleigh dissipation function are expressed for generalized coordinates for a total system of equations (2, 3).

$$L(u_0, u_1) = \frac{1}{2} C_1 (u_1)^2 \tag{2}$$

$$F(u_0, u_1) = \frac{1}{2} G_0 (u_0)^2 + \frac{1}{2} G_1 (u_0 - u_1)^2 \tag{3}$$

where:

u_0, u_1 — voltage on nodes 0 and 1 respectively,

G_0, G_1 — conductances,

C_1 — capacity.

By substituting derivatives of the Lagrangian (2) and Rayleigh dissipation function (3) into Lagrange's equation (1), we obtain the set of equilibrium equations for the nodes.

When the circuit is initially energized (charging part of the test without active gases) by a current source, the i_0 has a positive value. During the second step of the test without active gases when the fuel cell is disconnected from current source, there is no Lagrange equation for $k = 0$. During the last part of the test without active gases when the device is being discharged, the Lagrange equation for $k = 0$ appears but the sign of the i_0 current is negative.

The Lagrangian and Rayleigh dissipation function (Eqs. 4 and 5) are formulated for linear parameters of lumped elements. Mutual capacitances between particular capacitors are not taken into account. Mutual capacitances and parameter nonlinearities will be analyzed in the future. Eqs. 4 and 4 are valid for capacitances and conductances as a function of the temperature and pressure. Temperature and pressure are not generalized coordinates (are not a degree of freedom) of the analyzed test without active gases.

A single branch circuit has only two electrical degrees of freedom. These are the voltage of node 0 and voltage of node 1. The Lagrangian L and Rayleigh dissipation function F for this circuit are as follows:

$$L\left(\dot{\xi}_0, \dot{\xi}_1, \xi_0, \xi_1\right) = \frac{1}{2} C_1 \left(\dot{\xi}_1\right)^2 \tag{4}$$

$$F\left(\dot{\xi}_0, \dot{\xi}_1\right) = \frac{1}{2} G_0 \left(\dot{\xi}_0\right)^2 + \frac{1}{2} G_1 \left(\dot{\xi}_0 - \dot{\xi}_1\right)^2 \tag{5}$$

where the generalized coordinates are as in Eq. 6.

$$\dot{\xi}_0 = u_0; \qquad \dot{\xi}_1 = u_1 \tag{6}$$

The derivatives of the Lagrangian and Rayleigh function with respect to first generalized coordinates are given by Eq. 7.

$$\frac{\partial L}{\dot{\xi}_0} = 0; \quad \frac{\partial L}{\xi_0} = 0; \frac{\partial F}{\dot{\xi}_0} = G_0 \dot{\xi}_0 + G_1 \left(\dot{\xi}_0 - \dot{\xi}_1\right) \tag{7}$$

The derivatives of the Lagrangian and Rayleigh function with respect to second generalized coordinates are given by Eq. 8.

$$\frac{\partial L}{\dot{\xi}_1} = C_1 \dot{\xi}_1; \quad \frac{\partial L}{\xi_1} = 0; \frac{\partial F}{\dot{\xi}_1} = -G_1 \left(\dot{\xi}_0 - \dot{\xi}_1\right) \tag{8}$$

The set of the equilibrium is given by Eqs. 9 and 10.

$$G_0 \dot{\xi}_0 + G_1 \left(\dot{\xi}_0 - \dot{\xi}_1\right) = i_0(t) \tag{9}$$

$$C_1 \frac{\partial \dot{\xi}_1}{\partial t} - G_1 \left(\dot{\xi}_0 - \dot{\xi}_1\right) = 0 \tag{10}$$

After substituting the coordinates defined in Eq. 7 into Eqs. 9 and 10, the final form of the equilibrium equations is obtained, as shown in Eqs. 11 and 12.

$$G_0 u_0 + G_1 (u_0 - u_1) = i_0(t) \tag{11}$$

$$C_1 \frac{\partial u_1}{\partial t} - G_1 (u_0 - u_1) = 0 \tag{12}$$

The obtained system is interesting as it is an algebraic-differential set of equations. This type of equation requires a suitable solver, so a better approach is to transform these equations into a single differential equation. The first algebraic equation can be reformulated, leading to Eqs. 13, 14 and 15.

$$(G_0 + G_1)\, u_0 - G_1 u_1 = i_0(t) \tag{13}$$

$$(G_0 + G_1)\, u_0 = i_0(t) + G_1 u_1 \tag{14}$$

$$u_0 = \frac{1}{G_0 + G_1} i_0(t) + \frac{G_1}{G_0 + G_1} u_1 \tag{15}$$

This form allows u_0 to be replaced in the differential equation (21) with the derived expression. This process is illustrated in Eqs. 16, 17, 18, 19 and 20.

$$C_1 \frac{\partial u_1}{\partial t} + G_1 u_1 - G_1 \left(\frac{1}{G_0 + G_1} i_0(t) + \frac{G_1}{G_0 + G_1} u_1 \right) = 0 \tag{16}$$

$$C_1 \frac{\partial u_1}{\partial t} = \frac{G_1}{G_0 + G_1} i_0(t) + \frac{G_1^2}{G_0 + G_1} u_1 - G_1 u_1 \tag{17}$$

$$C_1 \frac{\partial u_1}{\partial t} = \frac{G_1}{G_0 + G_1} i_0(t) + \frac{G_1^2}{G_0 + G_1} u_1 - \frac{G_0 + G_1}{G_0 + G_1} G_1 u_1 \tag{18}$$

$$C_1 \frac{\partial u_1}{\partial t} = \frac{G_1}{G_0 + G_1} i_0(t) + \frac{G_1^2}{G_0 + G_1} u_1 - \frac{G_0 G_1 + G_1^2}{G_0 + G_1} u_1 \tag{19}$$

$$C_1 \frac{\partial u_1}{\partial t} = \frac{G_1}{G_0 + G_1} i_0(t) - \frac{G_0 G_1}{G_0 + G_1} u_1 \tag{20}$$

This leads us to a reduction of the system to a single differential equation. Of course, when the solver finds the solution, the u_0 need to be calculated using the appropriate formula.

2.2.1 Parameters identification method

To investigate the electric behavior of the tested FCs under varying thermal conditions, a series of controlled experiments was designed and executed. The following section describes the experimental methodology employed to carry out these measurements. Five measurements were performed using the test without active gases procedure described in more detail in [25]. Each of the measurements was performed for a different temperature in the range from 40°C to 120°C. In accordance with the results presented in [25], between each of the measurements a procedure of flushing the test bench with nitrogen was performed. This procedure was used to get rid of any remnants of air which could lead to measurement of remnant voltage. Each of the measurements consisted of three parts:

- Charging the cell with a constant current of 1 mA for a duration of 300 s,
- Self-discharge under open-circuit conditions, with an imposed current of 0 mA for 20 s,
- Forced discharge with a constant current of 5 mA until the measured voltage was reduced to 0 mV.

The complete test procedure is presented in the form of a block diagram in Fig. 3.

The procedure for identifying parameters R_0, R_1, and $C1$ adopted in this work is as follows. First, boundary conditions were established, defining the maximum and minimum allowable values for each parameter. The corresponding parameter ranges were then discretized to create a set of candidate values for R_0, R_1, and $C1$. Subsequently, all possible combinations of these discrete parameter values were systematically evaluated by numerically solving the governing differential equations for each set.

For each simulation result, a quality factor was computed to quantify the agreement between the model output and the experimental data. These quality factor values, together with the corresponding parameter sets, were stored for analysis. Finally, the stored data were examined to identify the parameter combination yielding the minimum quality factor value, thereby determining the optimal values of R_0, R_1, and $C1$ for the model.

2.3. Experimental setup

For the purpose of the experiments, a newly manufactured high-temperature PEM membrane-electrode assembly (MEA), featuring an active surface area of $25 cm^2$, was installed within the standard, expandable single-cell test fixture. The same type of MEA was used as described in the study by Gurau and De Castro (2020) [26]. To enable precise control of the electrical conditions during the experiments, a programmable power

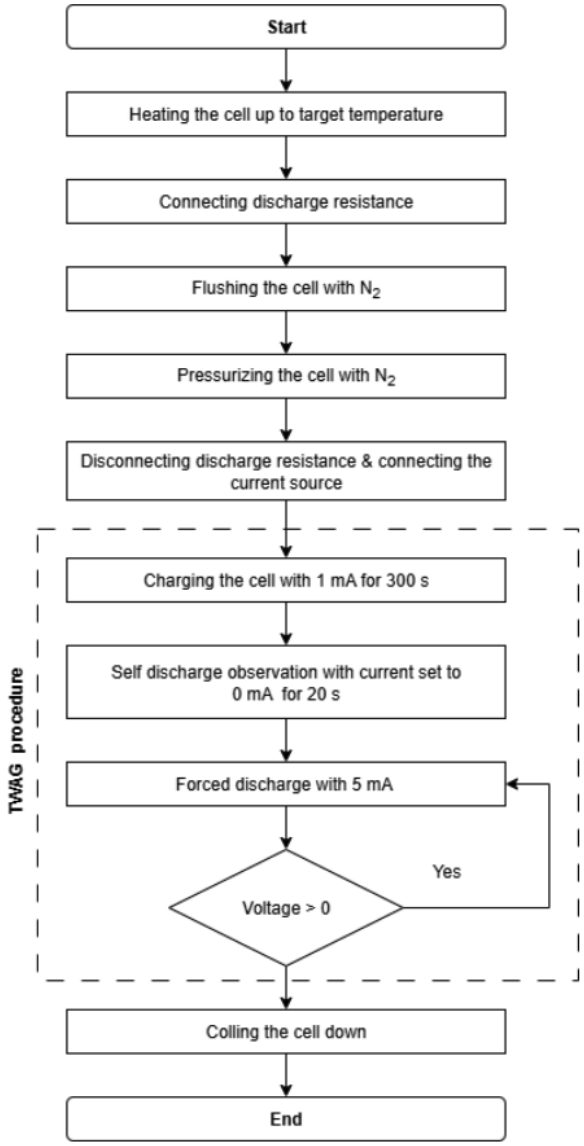

Figure 3: Test scenario for FC with no active gases.

supply operating in constant current mode—external to the main test bench system—was connected to the single cell. This external source was utilized to perform both charging and discharging cycles of the fuel cell under controlled conditions.

A schematic representation of the experimental test bench setup is shown in Fig. 4, illustrating the configuration and interconnections of the measurement and control equipment employed in this study.

All measurements presented in this article were conducted using a specialized test bench designed for the study of single-cell fuel cells. The test bench was fully automated and equipped with electrical heating, a cooling fan, mass flow controllers for nitrogen, hydrogen, and air, as well as an active load. For the purposes of the experiments described in this article, the active load was

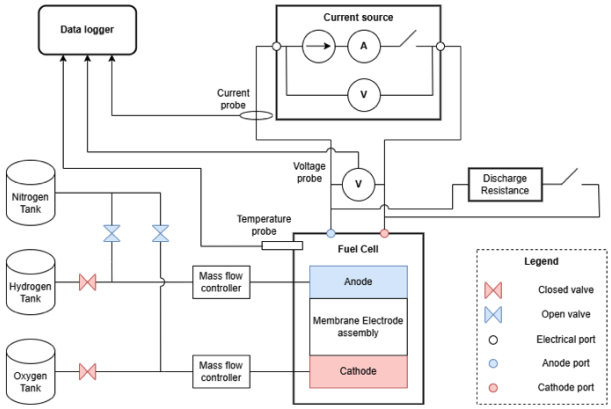

Figure 4: Schematic diagram of the experimental test bench setup showing measurement and control equipment configuration.

disconnected.

3. Results

3.1. Estimation of parameters

Fig. 5 presents values of the parameters R_0, R_1, C_1 found by the aforementioned parameter identification procedure for test without active gases curves measured for temperatures ranging from 40°C to 120°C, all performed at a nitrogen pressure of 1.2 atm at the start of the test. The correlation between the temperature of the test without active gases and the behavior of the cell is confirmed by the parameters found. There is a clear correlation between the temperature and model parameters R_0 and C_1. The observed influence of parameter R_1 is less apparent. As these measurements were done to confirm the topology of the proposed model, the authors did not further investigate this correlation. A further study aimed at modeling the parameters R_0 and C_1 as functions of temperature is proposed as further evolution of the model described in this work. In such a case, the study should be performed with more curves measured at a stable atmosphere with a smaller temperature difference between tests. The resistance R_o can be described as:

$$R_o(T) = -0.375 \cdot T + 86.7 \qquad (R = 0.8724) \quad (21)$$

where T is the temperature in degrees Celsius.

Similarly, the capacitance C_1 shows a linear increase with temperature and can be expressed as:

$$C_1(T) = 0.009 \cdot T + 2.9 \qquad (R = 0.8926) \quad (22)$$

In comparison to the capacity values presented in the literature [14, 15] for low temperature PEM fuel cells, the capacitance is higher but not by more than one order of

magnitude. This difference could be attributed to the different material used as the electrolyte.

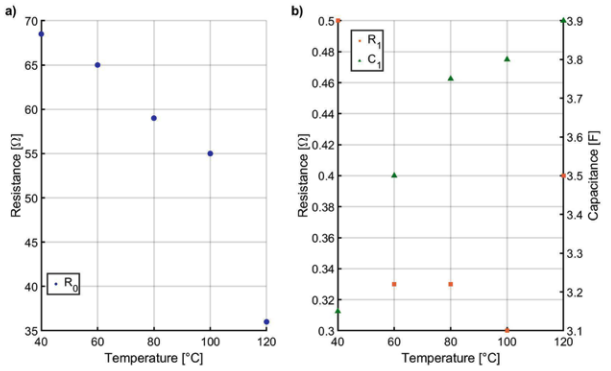

Figure 5: Identified model parameters from test without active gases measurements at 40˜120 °C and 1.2 atm nitrogen pressure: a) R_0, b) R_1 and C_1.

The simulation-estimated resistance, referred to as R_o, indicates a significant influence of fuel cell operating conditions on the overall ohmic resistance of the system. In studies involving membranes based on polybenzimidazole doped with phosphoric acid, the resistance increase under low humidity is significantly lower (+20–50%) [27], indicating higher stability under dry operating conditions. Additionally, poor interfacial contact between the catalytic electrode layer—typical for HT-PEMFCs operating at lower temperatures—and the membrane can lead to an increase in resistance in the range of +20–100% [28], and in some cases even higher. Notably, the occurrence of poor interfacial contact may cause a cumulative increase in resistance reaching up to +200–300% of the initial value [28, 29]. Such effects are likely present in the analyzed system, as evidenced by a noticeable increase in resistance observed during measurements. Therefore, the obtained results align with previously reported degradation mechanisms and provide a foundation for further research into HT-PEMFC diagnostic methods and the development of materials used in fuel cell systems.

3.2. Model validation

A comparison of the measurement waveform for these temperatures and the simulation waveform is presented in Fig. 6. A clear correlation between the temperature and the maximum value of the fully charged cell is clearly visible.

The quality factor was taken using the root mean square method RMSE. The RMSE is calculated as:

$$RMSE = \sqrt{\frac{\sum_{i=1}^{N} \left(u_i^{\text{ref}} - u_i^{\text{sim}}\right)^2}{N}} \tag{23}$$

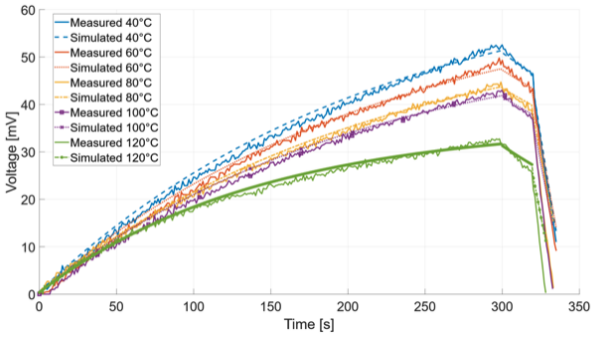

Figure 6: FC experimental data and simulation results during test without active gases measured at 1.2 atm for temperatures ranging from 40°C to 120°C.

where:

u_i^{ref} — i-th point of the measured waveform,
u_i^{sim} — i-th point of the simulated waveform,
N — number of data points that were compared.

The calculated RMSE values suggests that the fit was satisfactory. The shape of forced discharge curves plays a major part in these values, as can be seen based on the example of curves measured for 80°C and 100°C. The authors suggest that this can be explained by the fact that the current limitation of the current sources used was not precise enough. In future, the introduction of a current measurement redundancy in the form of an additional ammeter is advised.

As shown by Eq. 23, two identical waveforms would have zero value for the RMSE quality factor. The lower the value of this parameter, the better. During the study of parameters, the goal would be to achieve the lowest possible value. The RMSE values calculated for each test without active gases measurement as a function of temperature (40–120°C) are presented in Fig. 7. The RMSE values range from approximately 1.12 mV to 2.08 mV, indicating generally good agreement between the simulated and measured data.

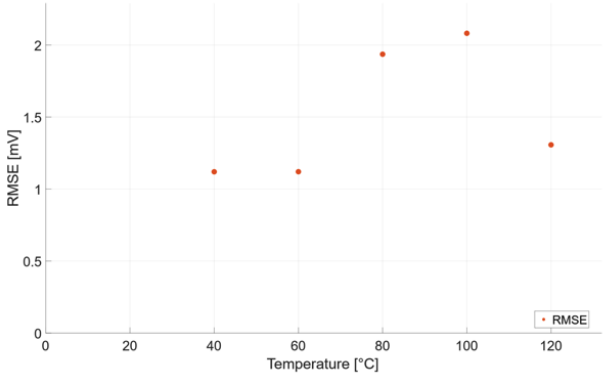

Figure 7: RMSE values calculated for each performed test without active gases as a function of temperature.

4. Conclusions

The proposed model provides a more than satisfactory fit to the measured curves for how little computational power it requires. This also shows promise for further development of the model and the test without active gases procedure.

The author suggests that following theoretical steps should be performed to further augment the model:

- Increase the number of RC branches,
- Introduce nonlinear capacity to the RC branch,
- Introduce parameters as functions of temperature $R_0(T)$ and $C_1(T)$.

Further experimental studies would be also advised, in particular testing the test without active gases methodology and the model for different types of fuel cells such as low temperature PEMFCs, SOFCs and MCFCs, etc.

For practical implementation of the results, the key action required would be to recreate the experiment and parameter identification presented in this work on a purposefully damaged fuel cell. This way the connection between the parameter values and damage could be examined and if such a connection was found, ranges of parameters of "healthy" and "faulty" fuel cells could be prepared.

References

[1] N. A. Qasem and G. A. Abdulrahman, "A recent comprehensive review of fuel cells: history, types, and applications," *International Journal of Energy Research*, vol. 2024, no. 1, p. 7271748, 2024.

[2] D. Chen, Z. Chen, K. Chang, R. Guo, S. Hu, P. Pei, and X. Xu, "A review on hydrogen supply subsystem of proton exchange membrane fuel cell system: Configuration, core components, theoretical model, and control strategy," *International Journal of Hydrogen Energy*, vol. 133, pp. 38–62, 2025.

[3] D. Karkosiński, W. A. Rosiński, P. Deinrych, and S. Potrykus, "Onboard energy storage and power management systems for all-electric cargo vessel concept," *Energies*, vol. 14, no. 4, p. 1048, 2021.

[4] I. Sebbani, M. K. Ettouhami, and M. Boulakhbar, "Fuel cells: A technical, environmental, and economic outlook," *Cleaner Energy Systems*, p. 100168, 2025.

[5] B. Hu, Z. Qu, and W. Tao, "A comprehensive system-level model for performance evaluation of proton exchange membrane fuel cell system with dead-ended anode mode," *Applied Energy*, vol. 347, p. 121327, 2023.

[6] R. Stropnik, A. Lotrič, A. Bernad Montenegro, M. Sekavčnik, and M. Mori, "Critical materials in PEMFC systems and a LCA analysis for the potential reduction of environmental impacts with EoL strategies," *Energy Science & Engineering*, vol. 7, no. 6, pp. 2519–2539, 2019.

[7] M. İnci and U. Aydemir, "Maximum power harvesting from fuel cell systems: A comprehensive review on critical role of MPPT methods, parameters and control algorithms," *International Journal of Hydrogen Energy*, vol. 138, pp. 823–842, 2025.

[8] S. Potrykus, J. Nieznański, F. Kutt, and F. J. Fernandez-Morales, "Modeling the effect of external load variations on single, serie and parallel connected microbial fuel cells," *Bioresource Technology*, vol. 416, p. 131761, 2025.

[9] K. Bharath, F. Blaabjerg, A. Haque, and M. A. Khan, "Model-based data driven approach for fault identification in proton exchange membrane fuel cell," *Energies*, vol. 13, no. 12, p. 3144, 2020.

[10] "A review of polymer electrolyte fuel cells fault diagnosis: Progress and perspectives, author=Zhou, Shangwei and Jervis, Rhodri, journal=Chemistry-Methods, volume=4, number=1, pages=e202300030, year=2024, publisher=Wiley Online Library,"

[11] S. Xiong, Z. Wu, and J. Cheng, "Design of a fuel cell test system with fault identification," *Electronics*, vol. 12, no. 15, p. 3365, 2023.

[12] S. Page, S. Krumdieck, and A. Anbuky, "Testing procedure for passive fuel cell state of health," in *Proc. Australia. Univ. Power Eng. Conf*, 2004.

[13] J. Aubry, N. Y. Steiner, S. Morando, N. Zerhouni, and D. Hissel, "Fuel cell diagnosis methods for embedded automotive applications," *Energy Reports*, vol. 8, pp. 6687–6706, 2022.

[14] H. Ashraf, M. M. Elkholy, S. O. Abdellatif, and A. A. El-Fergany, "Accurate emulation of steady-state and dynamic performances of pem fuel cells using simplified models," *Scientific Reports*, vol. 13, no. 1, p. 19532, 2023.

[15] N. Fouquet, "Real time model-based monitoring of a pem fuel cell flooding and drying out," in *2010 IEEE Vehicle Power and Propulsion Conference*, pp. 1–8, IEEE, 2010.

[16] S. C. Page, A. H. Anbuky, S. P. Krumdieck, and J. Brouwer, "Test method and equivalent circuit modeling of a pem fuel cell in a passive state," *IEEE Transactions on Energy Conversion*, vol. 22, no. 3, pp. 764–773, 2007.

[17] I. S. Martín, A. Ursúa, and P. Sanchis, "Modelling of pem fuel cell performance: Steady-state and dynamic experimental validation," *Energies*, vol. 7, no. 2, pp. 670–700, 2014.

[18] Conway, B. E. Electrochemical Supercapacitors. (Springer US, Boston, MA, 1999). doi:10.1007/978-1-4757-3058-6.

[19] T. J. Freeborn, B. Maundy, and A. S. Elwakil, "Fractional-order models of supercapacitors, batteries and fuel cells: a survey," *Materials for Renewable and Sustainable Energy*, vol. 4, no. 3, p. 9, 2015.

[20] Z. Cabrane and S. H. Lee, "Electrical and mathematical modeling of supercapacitors: Comparison," *Energies*, vol. 15, no. 3, p. 693, 2022.

[21] R. Vetter and J. O. Schumacher, "Free open reference implementation of a two-phase pem fuel cell model," *Computer Physics Communications*, vol. 234, pp. 223–234, 2019.

[22] M. Krpan, I. Kuzle, A. Radovanović, and J. V. Milanović, "Modelling of supercapacitor banks for power system dynamics studies," *IEEE transactions on power systems*, vol. 36, no. 5, pp. 3987–3996, 2021.

[23] S. Vlase, M. Marin, and N. Iuliu, "Finite element method-based elastic analysis of multibody systems: a review," *Mathematics*, vol. 10, no. 2, p. 257, 2022.

[24] M. A. Jarchlouei, A. Chitsaz, S. Mahmoudi, M. A. Rosen, and S. H. Bafekr, "Gibbs energy minimization using lagrange method of undetermined multipliers for electrochemical and thermodynamic modeling of a mcfc with internal steam reforming," *Energy Conversion and Management*, vol. 228, p. 113594, 2021.

[25] W. Rosiński, C. Turpin, and A. Wilk, "Influence of temperature and nitrogen pressure on the test without active gases for high-temperature proton exchange membrane fuel cells," *Archives of Electrical Engineering*, vol. 72, no. 3, 2023.

[26] V. Gurau and E. S. De Castro, "Prediction of performance variation caused by manufacturing tolerances and defects in gas diffusion electrodes of phosphoric acid (pa)–doped polybenzimidazole (pbi)-based high-temperature proton exchange membrane fuel cells," *Energies*, vol. 13, no. 6, p. 1345, 2020.

[27] J. Escorihuela, Ó. Sahuquillo, A. García-Bernabé, E. Giménez, and V. Compañ, "Phosphoric acid doped polybenzimidazole (PBI)/zeolitic imidazolate framework composite membranes with significantly enhanced proton conductivity under low humidity conditions," *Nanomaterials*, vol. 8, no. 10, p. 775, 2018.

[28] Q. Meyer, C. Yang, Y. Cheng, and C. Zhao, "Overcoming the electrode challenges of high-temperature proton exchange membrane fuel cells," *Electrochemical Energy Reviews*, vol. 6, no. 1, p. 16, 2023.

[29] N. Li, S. L. Sahlin, M. Zhou, V. Liso, and S. S. Araya, "Effects of operation modes on high temperature pem fuel cell stack degradation," *Next Energy*, vol. 3, p. 100118, 2024.